Supporting Information

Gianni et al. 10.1073/pnas.1405233111

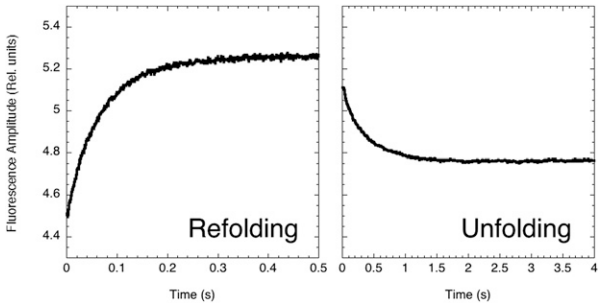

Fig. S1. Representative refolding and unfolding transitions in frataxin monitored by fluorescence. The transitions were initiated by rapid dilution of the denatured (refolding) and native (unfolding) frataxin in the appropriate buffer and recorded with a 320-nm cutoff filter with excitation wavelength of 280 nm. At all of the experimental conditions time course traces were consistent with a single exponential decay.

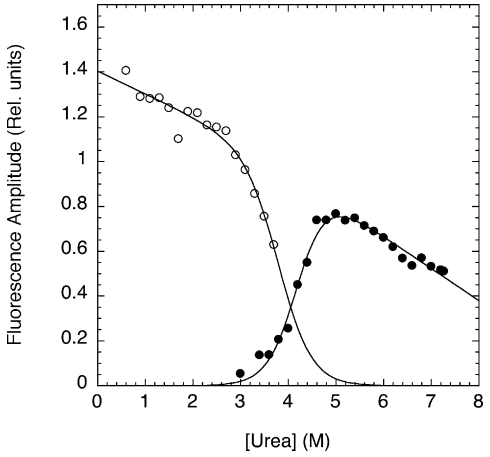

Fig. S2. Amplitude analysis of frataxin folding kinetics. The unfolding (●) and refolding (○) amplitudes are reported as a function of urea concentration. The lines are the best fit to a two-state equilibrium transition. As described in the main text, absence of burst-phase intermediates, as well as the agreement between the observed transition midpoints and *m* values, support the broad barrier model for the folding of frataxin.

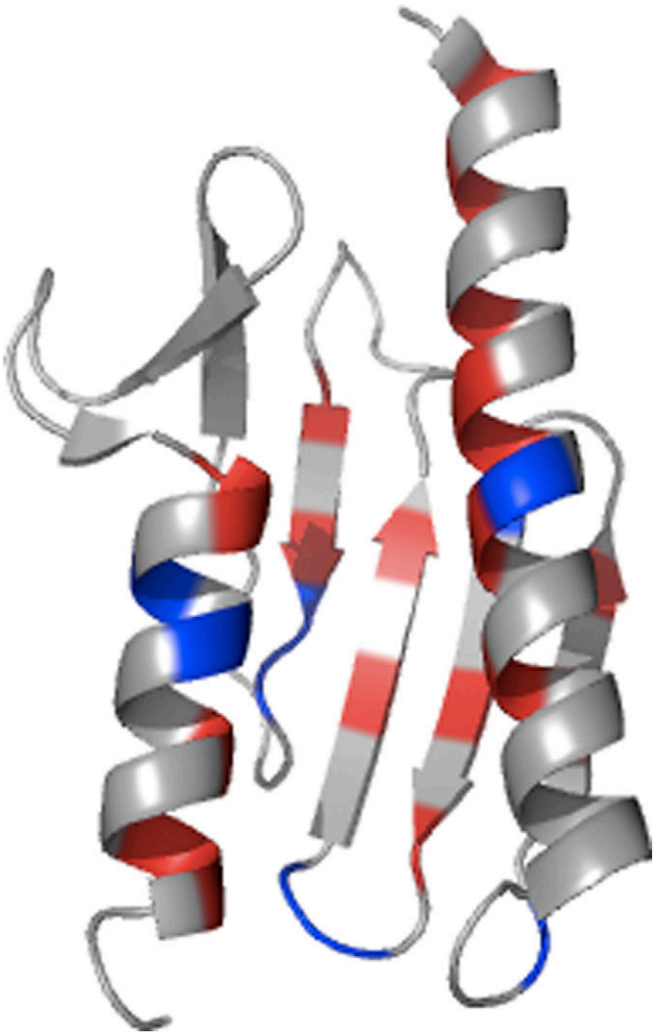

Fig. S3. Illustration of the positions of frataxin investigated by mutagenesis. The residues mutated in the first round (red) and in the second round (blue) of mutagenesis are highlighted on the structure. For clarity, the N-terminal tail of the first 15 residues of frataxin, which is disordered in the native state, is now shown.

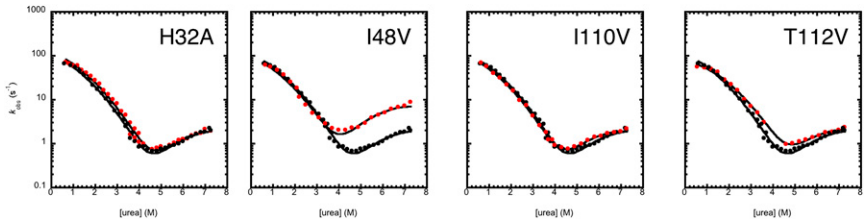

Fig. S4. Validation of the transition state structure by a second round of mutagenesis. The chevron plot of the mutants H32A, I48V, I110V, and T112S compared with that of wild-type frataxin. In each plot the mutant protein is represented by red circles and the wild-type protein by black circles. As described in the text, in the second round of mutagenesis we designed two group of mutants: the first one in the misfolded regions in the early transition state with $\beta_T = 0.45$ and the second (reported in this figure) in regions that were not forming any contacts. Consistently, none of the mutants displayed any effect on the folding rate constants, with three mutants nearly identical to the wild-type protein and one, I48V, displaying a $\Phi = 0$.

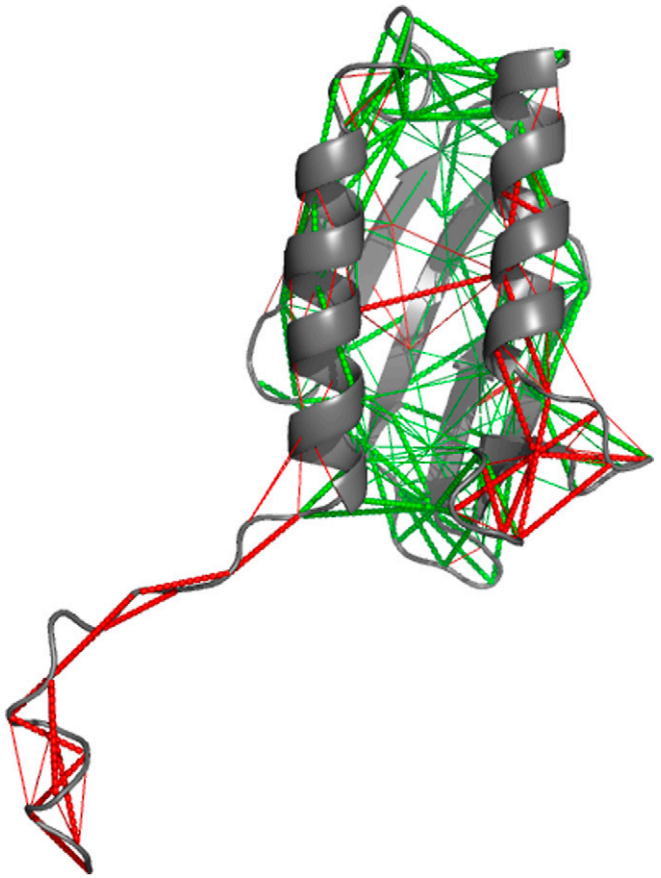

Fig. S5. Illustration of the frustrated interactions in the native state of frataxin. The frustration profile of frataxin was calculated from the frustratometer server (www.frustratometer.tk). The frustrated and nonfrustrated interactions are shown as red and green lines, respectively, and mapped on the structure of frataxin.

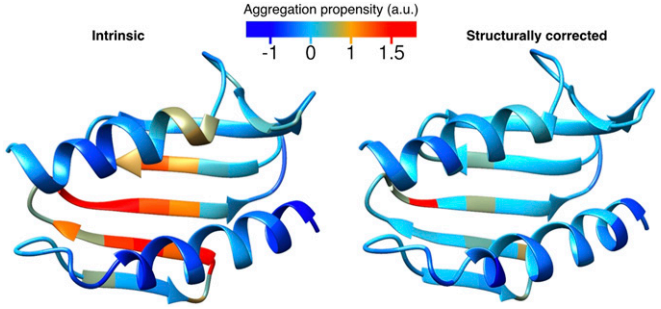

Fig. S6. Aggregation propensity of frataxin. (*Left*) The "intrinsic" aggregation propensity was calculated at a residue level using the Zyggregator method and mapped on the structure (1, 2). (*Right*) The "structurally corrected" aggregation propensity using Zyggregator method by taking into account the native structure of the protein, as described in ref. 3. A color-coded representation ranging from red (high propensity to aggregate) to yellow (weak propensity to aggregate), light blue (no propensity to aggregate), and blue (protected from aggregation) has been used.

1. Tartaglia GG, Vendruscolo M (2008) The Zyggregator method for predicting protein aggregation propensities. *Chem Soc Rev* 37(7):1395–1401.
2. Tartaglia GG, Vendruscolo M (2010) Proteome-level interplay between folding and aggregation propensities of proteins. *J Mol Biol* 402(5):919–928.
3. Tsytlonok M, Sormanni P, Rowling PJ, Vendruscolo M, Itzhaki LS (2013) Subdomain architecture and stability of a giant repeat protein. *J Phys Chem B* 117(42):13029–13037.

Fig. S7. Representation of the negatively charged surface of frataxin. Because of its function, frataxin displays a high content of negatively charged residues on its surface. These residues, which are highlighted in red sticks, modulate the stability of frataxin (1) and are involved in the binding of the different metals.

1. Sanfelice D, et al. (2014) Yeast frataxin is stabilized by low salt concentrations: Cold denaturation disentangles ionic strength effects from specific interactions. *PLoS ONE* 9(5):e95801.

Table S1. Measured change in free energy of unfolding upon mutation ($\Delta\Delta G_{D\text{-}N}$) and calculated Φ values at $\beta_T = 0.45$, 0.65, and 0.85

			Φ values		
Protein	$\Delta\Delta G_{D-N}$[†], kcal·mol^{-1}	$\Delta\Delta G_{D-N}$[‡], kcal·mol^{-1}	$\beta_T = 0.45$	$\beta_T = 0.65$	$\beta_T = 0.85$
L19A	1.5 ± 0.2	1.7 ± 0.1	−0.14 ± 0.03	0.22 ± 0.05	0.37 ± 0.09
Y22A	>4[§]	6.0 ± 0.3	0.13 ± 0.01	0.37 ± 0.03	0.46 ± 0.05
A26G	>4[§]	5.2 ± 0.2	0.08 ± 0.03	0.31 ± 0.07	0.37 ± 0.14
Y29A	1.5 ± 0.1	1.6 ± 0.1	0.01 ± 0.04	−0.02 ± 0.05	−0.01 ± 0.05
L30A	2.3 ± 0.3	2.1 ± 0.1	0.19 ± 0.03	0.35 ± 0.09	0.72 ± 0.24
L33A	>4[§]	4.4 ± 0.2	0.14 ± 0.01	0.50 ± 0.02	0.66 ± 0.05
L37A	3.8 ± 0.5	3.3 ± 0.2	0.18 ± 0.03	0.42 ± 0.06	0.76 ± 0.08
V51A	2.0 ± 0.3	2.1 ± 0.1	0 ± 0.01	0.01 ± 0.01	0.24 ± 0.10
L53A	2.5 ± 0.3	2.4 ± 0.1	0.03 ± 0.01	0.05 ± 0.02	0.22 ± 0.02
L60A	2.1 ± 0.3	2.0 ± 0.1	0.47 ± 0.02	0.68 ± 0.03	0.83 ± 0.06
I62V[¶]	0.4 ± 0.2	0.25 ± 0.07			
Y68A	>4[§]	4.3 ± 0.3	0.26 ± 0.05	0.33 ± 0.10	0.35 ± 0.11
I70V	1.0 ± 0.3	1.2 ± 0.05	0.35 ± 0.01	0.35 ± 0.02	0.42 ± 0.08
I79V	2.7 ± 0.2	2.4 ± 0.1	0.22 ± 0.02	0.29 ± 0.02	0.42 ± 0.06
L81A	3.1 ± 0.3	2.7 ± 0.2	0.39 ± 0.03	0.47 ± 0.09	0.47 ± 0.18
L107A	1.4 ± 0.2	1.9 ± 0.2	−0.02 ± 0.01	0.07 ± 0.03	0.34 ± 0.10
T108S[¶]	0.2 ± 0.2	0.4 ± 0.2			
V115A	1.4 ± 0.3	1.6 ± 0.1	0.18 ± 0.02	0.33 ± 0.04	0.71 ± 0.05
A118G	1.6 ± 0.2	1.9 ± 0.3	0.07 ± 0.01	0.06 ± 0.03	0.36 ± 0.03
I119V	1.1 ± 0.2	0.94 ± 0.1	0.14 ± 0.01	0.04 ± 0.3	−0.1 ± 0.04

Chevron plots were fitted globally to a quadratic equation, with a shared m_{total} value, as previously described (1, 2).
[†]Obtained from equilibrium experiments.
[‡]Obtained from kinetic experiments.
[§]Mutants were too unstable to observed a complete equilibrium transition. The mutant L111A expressed poorly and could not be characterized.
[¶]Mutants with $\Delta\Delta G_{D\text{-}N}$ too low (<0.4 kcal·mol^{-1}) to calculate a reliable Φ value (3).

1. Ternström T, Mayor U, Akke M, Oliveberg M (1999) From snapshot to movie: Phi analysis of protein folding transition states taken one step further. *Proc Natl Acad Sci USA* 96(26): 14854–14859.
2. Gianni S, Brunori M, Jemth P, Oliveberg M, Zhang M (2009) Distinguishing between smooth and rough free energy barriers in protein folding. *Biochemistry* 48(49):11825–11830.
3. Fersht AR, Sato S (2004) Phi-value analysis and the nature of protein-folding transition states. *Proc Natl Acad Sci USA* 101(21):7976–7981.

Table S2. Measured change in free energy of unfolding upon mutation ($\Delta\Delta G_{D\text{-}N}$) and calculated Φ values at $\beta_T = 0.45$, 0.65, and 0.85

			Φ values		
Protein	$\Delta\Delta G_{D-N}$[†], kcal·mol^{-1}	$\Delta\Delta G_{D-N}$[‡], kcal·mol^{-1}	$\beta_T = 0.45$	$\beta_T = 0.65$	$\beta_T = 0.85$
M58A	1.0 ± 0.4	1.26 ± 0.2	−0.1 ± 0.06	−0.53 ± 0.1	−0.2 ± 0.09
A64G	0.30 ± 0.2	0.50 ± 0.3	−0.53 ± 0.08	−2.37 ± 0.1	−1.89 ± 0.2
F65A	1.6 ± 0.2	1.46 ± 0.2	0.13 ± 0.05	0.07 ± 0.01	0.23 ± 0.08
A82G	−0.9 ± 0.4	−0.74 ± 0.2	−0.57 ± 0.06	−0.29 ± 0.1	−0.37 ± 0.2
S83A	1.0 ± 0.3	1.27 ± 0.3	0.12 ± 0.05	0.29 ± 0.08	1.18 ± 0.1

Chevron plots were fitted globally to a quadratic equation, with a shared m_{total} value, as previously described (1, 2). The mutants V57A and L85A expressed poorly and could not be characterized.
[†]Obtained from equilibrium experiments.
[‡]Obtained from kinetic experiments.

1. Ternström T, Mayor U, Akke M, Oliveberg M (1999) From snapshot to movie: phi analysis of protein folding transition states taken one step further. *Proc Natl Acad Sci USA* 96(26): 14854–14859.
2. Gianni S, Brunori M, Jemth P, Oliveberg M, Zhang M (2009) Distinguishing between smooth and rough free energy barriers in protein folding. *Biochemistry* 48(49):11825–11830.